Collimated Bidirectional Propagating Spin Wave Generated by a Nonlocal Spin-Current Nano-oscillator

Lina Chen,[1,2] Zhenyu Gao,[2] Kaiyuan Zhou,[2] Y.W. Du,[2] and R.H. Liu[2,*]

[1] *School of Science, Nanjing University of Posts and Telecommunications, Nanjing, 210023, China*

[2] *Jiangsu Provincial Key Laboratory for Nanotechnology, National Laboratory of Solid State Microstructures and School of Physics, Nanjing University, Nanjing, 210093, China*

(Received 8 April 2021; revised 9 July 2021; accepted 13 September 2021; published 24 September 2021)

Pure spin currents, generated by nonlocal spin injection and spin-orbit effects, have been widely used to control magnetization reversal and dynamics by current without charge transfer and its side effects in the device's actual working region. Here we experimentally demonstrate that a single coherent spin-wave mode can be excited by the pure spin current in a nonlocal spin-injection spin-valve device. The microwave spectra show that the observed spin-wave frequency is higher than the ferromagnetic resonance frequency, and almost does not change with the excitation current at moderate magnetic fields, indicating that the observed dynamical mode is a linear propagating spin-wave mode. Furthermore, micromagnetic simulations based on our device geometry generally reproduce the experimentally observed field-dependent and current-dependent oscillation characteristics, and provide us with the additional spatial information that the spin-wave mode exhibits collimated and bidirectional propagation paths in the direction perpendicular to the applied magnetic field. Our simulation results also show that the current-local Oersted field in our nonlocal device is much smaller than in conventional nanocontact magnetic oscillators, and has a minimal impact on the spin-wave dynamics. A near-symmetrically-collimated and bidirectional propagating spin-wave beam with magnetic field–controllable beam direction and current-independent frequency, achieved in our demonstrated nonlocal spin-current nano-oscillator, can be used as a local spin-wave source for magnonic logic devices and can be used to build daisy-chaining oscillatory neural networks with mutual synchronization.

DOI: 10.1103/PhysRevApplied.16.034044

I. INTRODUCTION

Recent manipulation of magnetization reversal and control of dynamics using pure spin currents generated by the spin-orbit effects (spin Hall, spin Seebeck, and interfacial Rashba effects) in bilayers of ferromagnets with heavy nonmagnetic metals or topological materials have demonstrated that pure spin currents are anticipated to revolutionize electronics [1–6]. Before the spin-orbit effects, it was experimentally proved that a pure spin current can be efficiently generated by injecting a spin-polarized charge current by spatially separating charge and spin currents within lateral spin-valve structures, also named "nonlocal spin-injection devices" [7–12]. The pure spin current can transfer spin angular momentum without charge current, minimize charge current–induced Joule heating and Oersted field effects on the actual layer or region to avoid local heating and Oersted field-induced side effects [13,14], and achieve energy-efficient magnetic-random-access-memory and magnonic devices. Therefore, spin current–driven magnetization switching and modulation of magnetic damping in both nonlocal spin-injection and spin-orbit-torque devices have been intensely studied in recent years [15–18]. Additionally, since spin current–driven coherent magnetization dynamics can be used as a microscale or nanoscale microwave signal source or spin-wave source in a wide variety of applications, such as wire communications and analog neuromorphic computing, planar spin Hall nano-oscillators (SHNOs) with various materials and geometries have also received increased attention in recent years because of their simplicity and reproducibility [19–32]. Many spectroscopy experiments found that the abundant and distinct dynamical behaviors driven by the pure spin current in SHNOs are closely related to the geometry of spin-current injection and the magnetic properties of the free magnetic layer, differing from that of conventional spin-transfer-torque (STT) nano-oscillators (STNOs), where the spin current always flows together with the charge current through the magnetic multilayers and results in undesirable Joule heating and a significant local Oersted field [14,33–35]. However, substantial experiments and consistency regarding excitation

*rhliu@nju.edu.cn

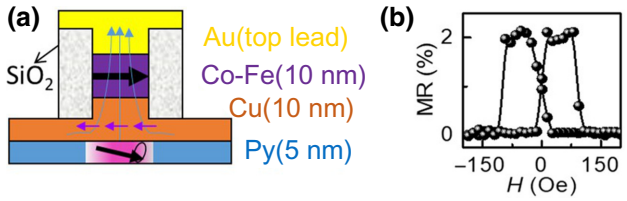

FIG. 1. (a) The stacked multilayer of the nonlocal spin-current nano-oscillator. The two bold arrows indicate the magnetization directions of the polarized and free layers. The thin arrows and the curves indicate the polarization and the flow direction of electrons, respectively. The diameter of the circular nanocontact is approximately 90 nm. (b) Magnetoresistance (MR) hysteresis loop measured with a small current $I = 0.1$ mA and an in-plane magnetic field.

of coherent magnetization dynamics by the spin current in nonlocal spin-valve devices are still lacking [36–39].

Here we experimentally study the dynamics of magnetization auto-oscillations based on a nanocontact nonlocal spin-valve structure. A single coherent spin-wave mode can be excited by the pure spin current. Its frequency is slightly higher than the ferromagnetic resonance (FMR) frequency f_{FMR} of the permalloy (Py) free layer, and remains almost constant with increasing excitation current at low magnetic fields $H \leq 1000$ Oe and undergoes a weak blueshift with increasing current at high fields $H \geq 1095$ Oe, in contrast to the localized "bullet" mode with a frequency much lower than f_{FMR} and a significant nonlinear frequency redshift observed in conventional STNOs and SHNOs with in-plane magnetization. Furthermore, the spatial mapping of this mode, obtained by micromagnetic simulation modeling from our experimental device's geometry, further confirms that the dynamical mode is a linear propagating spin-wave mode with collimated and bidirectional propagation paths in the direction perpendicular to the applied external magnetic field.

II. EXPERIMENT

A. Device fabrication and electronic characteristics

Figure 1(a) shows a schematic of the nonlocal spin-current nano-oscillator (NLSCNO) based on stacked magnetic multilayers. The device is based on a trilayer Py(5 nm)/Cu(10 nm)/$Co_{30}Fe_{70}$(10 nm) disk with 20-μm diameter deposited on an annealed sapphire substrate by magnetron sputtering. The spin-polarized $Co_{30}Fe_{70}$ layer and a half of the Cu space layer are processed into a circular nanopillar with a diameter of approximately 90 nm by a combination of electron-beam lithography and Ar-ion milling. The two Au electrodes are attached to the top surface of the circular Co-Fe nanopillar and the Cu space layer at the edge of a 20-μm-diameter Py(5 nm)/Cu(5 nm) disk, respectively. The electrodes are electrically insulated by a 30-nm-thick insulating SiO_2 layer. In this spin-valve structure, the magnetoresistance ratio is about 2% at room temperature [Fig. 1(b)], much smaller than the giant-magnetoresistance ratio of the conventional perpendicular spin-valve structure with the current flow fully perpendicular to the device plane. The reason is that most current passes through the extended Cu layer rather than the bottom Py free layer because the electrical conductivity of Cu is 10 times greater than that of Py. All the microwave-generation-spectra measurements described below are performed with an in-plane magnetic field at room temperature.

B. Spectral characteristics of the nonlocal spin current–driven dynamical mode

To experimentally explore the dynamical states of the Py layer induced by injection of spin current generated by spin diffusion in the Cu layer and spin accumulation at the Cu/Co-Fe interface, we perform spectroscopic measurements on the nonlocal spin-valve device with different in-plane magnetic fields H and excitation currents. In our all spectroscopic measurements, the magnetizations of both the Co-Fe layer and the Py layer are aligned by the applied static in-plane field H above the coercive field $H_c \sim 100$ Oe of the devices [see Fig. 1(b)]. To exert sufficient spin-transfer torque on the Py layer and excite its magnetization auto-oscillation, we need to generate the spin current with the spin magnetic moment antiparallel to the Py layer's magnetization by applying a positive electric current as defined in Fig. 1(a). Figure 2 shows representative auto-oscillation spectra acquired above the onset current I with field H ranging from 270 to 1175

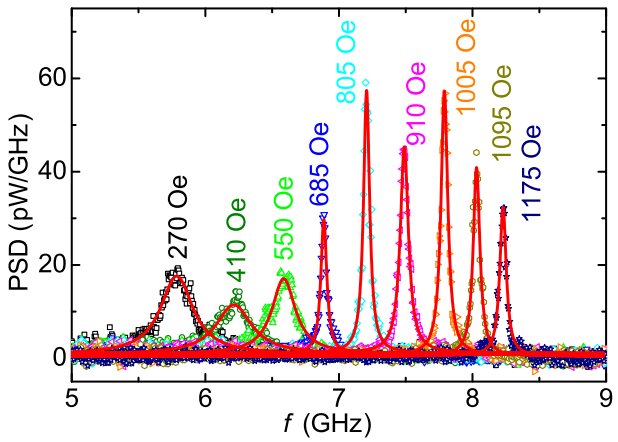

FIG. 2. Microwave-generation spectra (symbols) of the NLSCNO obtained above the onset excited current and at the labeled values of the magnetic fields H. The curves are the results of fitting with a Lorentzian function. PSD, power spectral density.

Oe. The spectral peaks, shown in Fig. 2, are well approximated by the Lorentzian function, as shown by the solid curves. No auto-oscillating peak is observed in all negative currents, consistent with the expected effects of STT produced by the nonlocal spin current on the dynamic damping, and in contrast to our previously studied vertical nanocontact–based spin Hall nano-oscillator (VNSHNO) [31], where, like positive currents, negative currents can also excite auto-oscillating magnetization because of the chiral symmetry of the spin-current polarization arising from the spin Hall effect in the VNSHNO structure.

The dependence of the oscillation characteristics on the excitation current can be used as a vital indicator to identify the mode of the spin wave excited in spin-torque nano-oscillators. In previous studies, the nonlinear self-localized "bullet" spin-wave mode with a frequency far below the spectrum of linear spin waves was usually observed in SHNOs [19,20,23,24,28] and conventional nanocontact STNOs (NCSTNOs) with in-plane magnetization [14,33]. This spin-wave "bullet" mode exhibits a significant redshift and thermal linewidth broadening with increasing excitation current due to nonlinearity [20,40–42]. To obtain further insight into the nature of the dynamical states in our NLSCNO, we investigate the dependence of the spectral characteristics on the excitation current I at different magnetic fields. Figure 3 shows pseudocolor maps of the current dependence of the microwave power spectral density generated by our device at various fields H. In contrast to the nonlinear spin-wave "bullet" mode with a distinct redshift of the frequency with increasing current, the observed current-dependent spectra show that the frequency of the auto-oscillator remains almost constant with increasing current at low magnetic fields $H \leq 1000$ Oe, indicating that the dynamical nonlinearity coefficient is much smaller than that of the "bullet" mode in the Py(5 mn)/Pt(4 nm)–based SHNO system [19,20] and the linear spin-wave modes localized in the potential well created by the spin current in the NCSTNO based on the extended $Co_{70}Fe_{30}$(8 nm)/Cu(20 nm)/Py(5 nm) disk [36,37]. At high fields $H \geq 1095$ Oe, the oscillation frequency gradually exhibits a weak blueshift with increasing current, which may be related to a considerable out-of-plane component of the magnetic field due to a slight deviation of the applied field from the film plane in our experiment because previous studies found that an out-of-plane orientation of magnetization could cause positive nonlinearity [33,42,43].

To gain further insight into the dynamical mode observed in our NLSCNO, we also analyze the dependence of the spectra on the magnetic field. Field-dependent spectral characteristics such as the full width at half maximum (FWHM), the central peak frequency f_c, and the generated power P are extracted from the Lorentzian fitting. To eliminate a possible contribution from current-dependent spectral characteristics, we focus on the field-dependent minimum linewidth of the dynamical mode, which coincides with the highest peak power spectral density at current I_p. Figure 3(k) shows that both I_p and the onset current I_c rapidly decrease by 43% as the applied magnetic field H increases from 270 to 1175 Oe, in opposition to the established models of spin torque–induced magnetization dynamics in conventional NCSTNOs [27,33] and SHNOs [19,20], where I_c increases with increasing H due to local viscous damping of the magnetization precession [44]. The

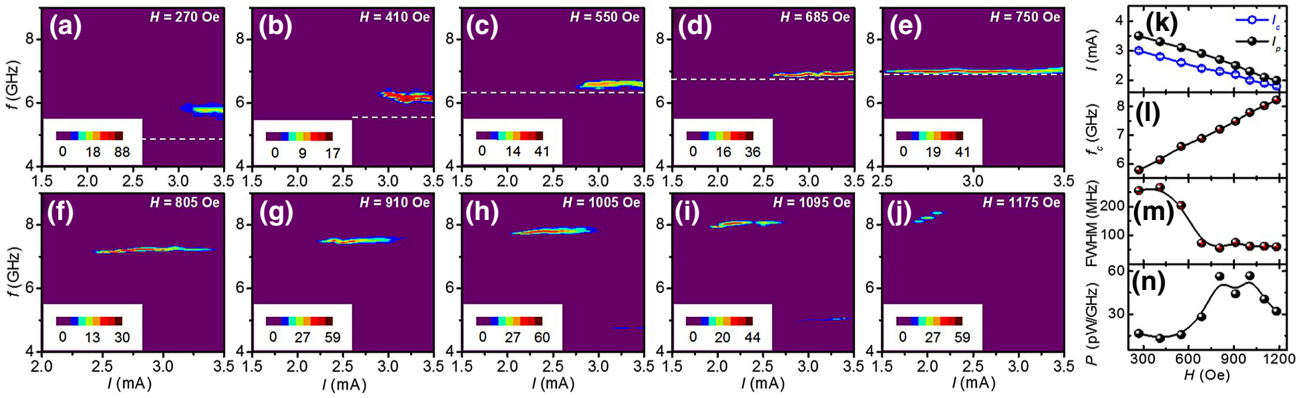

FIG. 3. Dependence of the microwave-generation characteristics on current at different magnetic fields H. (a)–(j) Pseudocolor plots of current-dependent spectra obtained at $H = 270$ Oe (a), $H = 410$ Oe (b), $H = 550$ Oe (c), $H = 685$ Oe (d), $H = 750$ Oe (e), $H = 805$ Oe (f), $H = 910$ Oe (g), $H = 1005$ Oe (h), $H = 1095$ Oe (i), and $H = 1175$ Oe (j). (k) Dependence of the onset current I_c (open circles) and the current corresponding to the highest peak power spectral density I_P (solid circles) on the external magnetic field H. (l)–(n) Dependence of the central generation frequency f_c (l), linewidth FWHM (m), and integral intensity P corresponding to the highest-intensity peak of the power spectral density at I_P (n) on H. f_c, FWHM, and P are determined by our fitting the power spectra in (a)–(j) with the Lorentzian function. The solid lines are given as guides for the eye. Dashed horizontal lines show the FMR frequency f_{FMR} of the Py layer.

observed anomalous field-dependent characteristic currents are related to the field-dependent STT efficiency between the Py free layer and the Co-Fe polarized layer. Unlike the previously reported NCSTNOs, the Co-Fe(10 nm) polarized layer of our NLSCNO is a quasi-free-layer without the pinning effect from an adjacent antiferromagnet layer. As shown in Fig. 1(b), the magnetoresistance loop shows that the coercive field of Co-Fe(10 nm) is only approximately 100 Oe, also suggesting a weak pinning effect with a negligible shape magnetic anisotropy because the circular Co-Fe nanopillar is rotationally symmetric. At high current density and low external magnetic fields, spin current excites magnetization precession of the extended Py(5 nm) and also drives deviation of the magnetization of Co-Fe(10 nm) from its equilibrium position, and in consequence reduces the STT efficiency with decreasing H. The broad linewidth FWHM and low peak power spectral density below 600 Oe [Figs. 3(m) and 3(n)] also support the above argument. Meanwhile, the current-induced considerable Oersted field located at the Co-Fe layer can also significantly modulate the Co-Fe magnetization direction in the lower-field range and can reduce the STT efficiency from the polarized layer to the free layer. Besides, the frequency of the dynamical mode, observed in this nonlocal spin-valve structure (Fig. 3), is slightly higher than the FMR frequency of the Py layer, suggesting that this mode is a propagating spin wave.

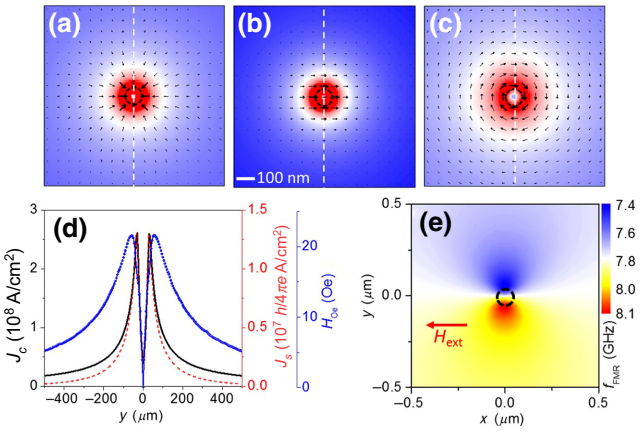

FIG. 4. Analysis of the distribution of the electrical current, spin current, and Oersted field in a nonlocal spin-current nano-oscillator. (a) Calculated spatial map of the electrical current density J_c in the extended Cu layer at $I = 3$ mA. (b) Calculated spatial map of the spin current density J_s injected from Cu into Py with consideration of the spin-diffusion length of 300 nm of Cu, where the arrows indicate the spin direction antiparallel to the magnetization direction of the Py layer. (c) Calculated spatial map of the in-plane Oersted field H_{Oe} in the Py layer at $I = 3$ mA. (d) Section of J_c (solid curve), J_s (dashed curve), and H_{Oe} (blue spheres) distributions along the y axis, as shown by the dashed lines in (a),(b),(c), respectively. (e) The FMR frequency landscape calculated by our taking into account the applied external field $H_{ext} = 805$ Oe and current-induced Oersted fields at $I = 3$ mA. The dashed circle marks the nanocontact.

III. SIMULATIONS

A. Calculation of nonlocal spin current and Oersted field

To further elucidate the nature of the observed dynamical mode, we perform micromagnetic simulations using OOMMF [45]. The simulation cell size is $5 \times 5 \times 5$ nm^3, and the simulated volume is a circular Py disk with a diameter of 3 μm and a thickness of 5 nm. The following material parameters are used in the simulations: exchange stiffness $A = 13$ pJ/m, saturation magnetization $M_s = 700$ kA/m, Gilbert damping constant $\alpha = 0.03$, and effective STT efficiency $P = 0.05$ [7,8]. Figures 4(a) and 4(b) show the electrical current and spin-current distributions of the Cu layer, which are numerically calculated by the COMSOL Multiphysics package [46] with resistivity of 0.27 $\mu\Omega$ m for the 5-nm-thick Py layer and 0.017 $\mu\Omega$ m for the Cu layer. Calculation of the current distribution shows that approximately 95% of the outflowing current drains through the 5-nm-thick residual Cu layer, and only approximately 5% passes through the 5-nm-thick Py layer, which supports a small giant-magnetoresistance ratio of approximately 2% as observed in Fig. 1(b). The radial electrical current and spin current with spin polarization along the y axis reach their largest values in the Cu layer near the edge of the nanocontact [Fig. 4(d)]. To more accurately calculate the spin-current distribution of our device, we also take account of the spatial decay of the spin polarization in the Cu layer by using an experimentally obtained spin-diffusion length $\lambda = 300$ nm [7]. From the results, the spin current is more localized than the electrical current [Fig. 4(d)]. We also calculate the position-dependent Oersted field from the current-density distribution. The radial current-induced chiral Oersted field in the Py layer has its maximum $H_{Oe} = 22$ Oe located on the circle with 120-nm diameter [Fig. 4(c)]. The spin current density decreases by about a factor of 2 within a distance of about 40 nm from the nanocontact edge, while the Oersted-field distribution is much less localized than that of the spin current.

To quantitatively analyze the effect of the local Oersted field on magnetic dynamics, we numerically calculate the spatial profile of f_{FMR} of the Py layer at a representative magnetic field $H_{ext} = 805$ Oe by using the well-known Kittel formula based on the calculated total magnetic field, including the Oersted field. The FMR frequency f_{FMR} is defined as $f_{FMR} = \gamma\sqrt{H_{tot}(H_{tot} + 4\pi M_s)}$, where γ is the gyromagnetic ratio and M_s is the saturation magnetization. Figure 4(e) shows the weak antisymmetric FMR frequency f_{FMR} landscape along the y axis caused by the circular Oersted field, which could promote preferential propagation paths for the generated spin wave [31,34,47]. Therefore, it

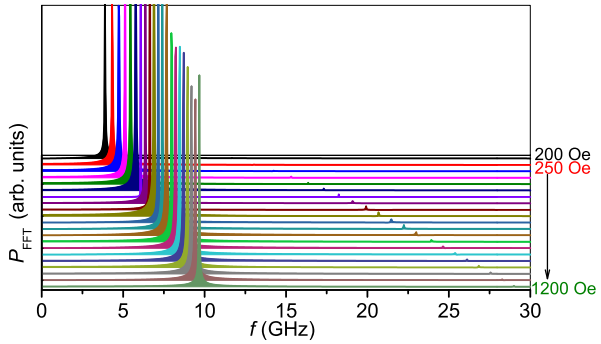

FIG. 5. Dependence of auto-oscillation spectra obtained by micromagnetic simulation on the magnetic field H from 200 to 1200 Oe increased in 50-Oe steps. The low-frequency peak with higher power intensity is the fundamental auto-oscillation mode, while the high-frequency peak is the third harmonic mode of auto-oscillation. FFT, fast Fourier transform.

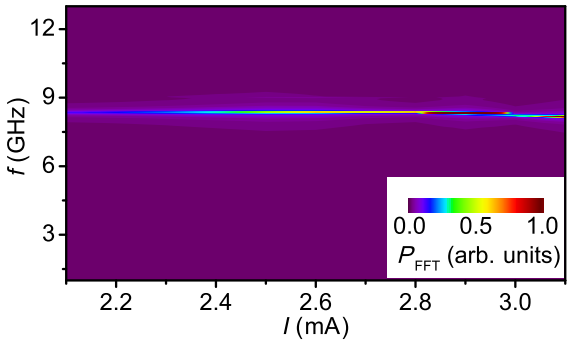

FIG. 6. Pseudocolor map of the calculated power spectral density as a function of excited current I at $H = 805$ Oe. FFT, fast Fourier transform.

is necessary to take the spin current and Oersted field into account in our micromagnetic simulations.

B. Dependence of power spectra on the magnetic field and current

Figure 5 shows micromagnetic simulations of current-induced magnetization dynamics, including the calculated circular-Oersted-field and spin-current distributions at different external magnetic fields, generally consistent with the experimentally observed microwave-generation spectra with a single oscillating peak in Fig. 2. The slight deviation in the frequency between simulated and experimentally observed values may be caused by the deviation of actual M_s and the stray field from the top Co-Fe(10 nm) nanopillar, which is not taken into account in the simulations. The third harmonic $3f$ is also observed in the calculated spectra due to the large amplitude of oscillation at sufficiently large currents. Higher-order harmonics are not experimentally observed, which may be because of our microwave spectroscopy's limited detection sensitivity. However, the physical mechanism of only odd-order harmonics rather than even-order harmonics is not clear yet, warranting further studies.

To gain more detailed information on the dynamical properties of this spin-current nano-oscillator, we further study the dependence of the calculated spectra on the excitation current I at a representative magnetic field $H = 805$ Oe. Figure 6 shows that auto-oscillation has a fundamental frequency $f_c = 8.35$ GHz higher than the calculated FMR frequency $f_{FMR} = 7.4$–8.1 GHz [Fig. 4(e)], and remains constant with increasing current above the onset current $I = 2.1$ mA. These results are also consistent with the experimental observations discussed for Fig. 3.

C. Spatial characteristics of the auto-oscillation mode

The spatial characteristics of the calculated auto-oscillation mode can also be accessed in our micromagnetic simulation. Figures 7(a)–7(d) show four representative snapshots of the distribution of instantaneous in-plane magnetization component M_y for excitation current $I = 3$ mA and $H = 805$ Oe, suggesting the oscillation period τ is approximately 0.12 ns. Furthermore, the Fourier spectrum [Fig. 7(f)], obtained by fast Fourier transform of the spatially averaged $M_y(t)$, shows that the oscillating magnetization's fundamental frequency is 8.35 GHz, confirming the oscillation period $\tau = 0.12$ ns. Meanwhile, the third harmonic is also observed in the calculated spectrum. Time sequences of M_y show a propagating spin-wave feature with a highly anisotropic propagation velocity and amplitude for parallel and vertical magnetic field directions, respectively [Figs. 7(a)–7(d)]. The section profiles of M_y at $t = 40$ ns further show that the spin-wave wavelength λ is 0.9 μm along the y axis and 0.3 μm along the x axis, and the oscillating amplitude of magnetization is also large along the y axis, suggesting that the spin-wave propagation path is preferentially in the direction perpendicular to the external magnetic field [Fig. 7(e)]. To obtain comprehensive information on the power distribution of the modes, we also calculate the normalized spatial power maps of the observed dynamical mode and its third harmonic, obtained from the time dependence of the local magnetization component m_y^2 by pointwise temporal fast Fourier transform over the simulated area. Figures 7(g) and 7(h) show that the fundamental and third-harmonic modes both exhibit a bidirectionally elongated spatial profile in the direction perpendicular to the applied magnetic field. Additionally, combined with the calculated spatial profile of the Oersted field above [Fig. 4(c)], we find that the largest power density is located on the upper side of the nanocontact, where the total magnetic field is the minimum due to the Oersted field opposite the applied magnetic field [Fig. 1(d)], suggesting the propagation direction of the spin wave is

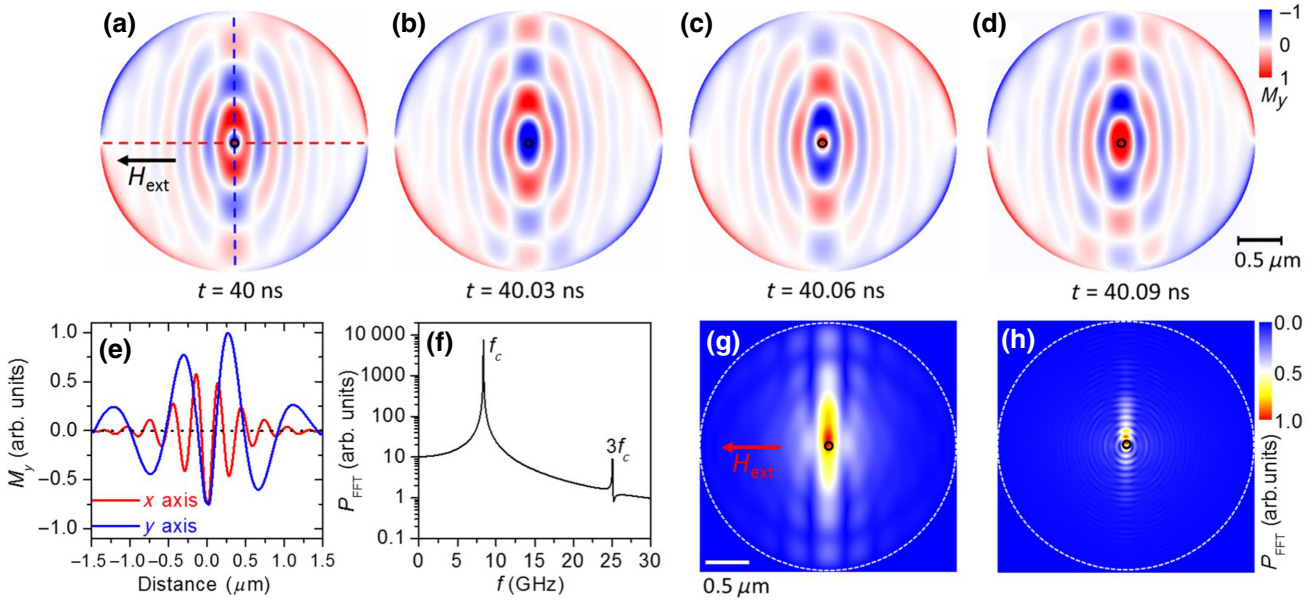

FIG. 7. Spatial characteristics of the auto-oscillation mode. (a)–(d) Time sequences of in-plane magnetization component M_y obtained from micromagnetic simulations at $I = 3$ mA and in-plane magnetic field $H = 805$ Oe. (e) Section of the magnitude of M_y at simulation time $t = 40$ ns along the y axis and the x axis, respectively, as shown by the dashed lines in (a). (f) Calculated auto-oscillation spectrum showing a single oscillating mode and its third harmonic obtained by fast Fourier transform (FFT) of the time-dependent M_y. (g),(h) Normalized spatial maps of the square of the simulated dynamical magnetization component M_y^2 of the fundamental mode $f = 8.35$ GHz (g) and its third-harmonic mode $3f = 25.05$ GHz (h). The large dashed circle represents the boundary of the active simulation region, the small dashed circle marks the top nanocontact, and the arrow shows the direction of the applied external field.

modified slightly by the weak local Oersted field. Unlike in previous studies of NCSTNOs [14,34], the strong Oersted field (approximately 1 kOe) causes a highly asymmetric propagation of spin waves by locally modifying the spectral frequency of spin waves of the extended magnetic films. Meanwhile, the current-induced local Oersted field may completely prevent spin waves from propagating by creating a deep potential well to localize or trap spin waves if it is strong enough and localized [14]. In our NLSCNO, the maximum Oersted field is 22 Oe for excitation current $I = 3$ mA, only about 2.7% of the uniform external magnetic field $H_{ext} = 805$ Oe [Fig. 4(d)]. The small Oersted field causes a relatively weak variation of ± 0.35 GHz (approximately 4.5% of 7.75 GHz) in the FMR-frequency landscape in the Py free layer [Fig. 4(d)], which is much smaller than the reported 3 GHz (approximately 17% of 18 GHz) in NCSTNOs [34]. Therefore, in contrast to the highly collimated and single-direction spin-wave beam observed in NCSTNOs, the propagating spin-wave beam in our NLSCNO is a collimated and bidirectional beam with a weak asymmetric amplitude along the $\pm y$ axis perpendicular to the external field because the current-induced local Oersted field in the actual oscillating layer can be minimized in our modulated nonlocal spin-current nano-oscillator.

IV. CONCLUSION

In summary, our experiment and numerical simulation demonstrate a linear propagating spin-wave excitation in a NLSTNO based on planar nonlocal spin injection. Differing from a localized spin wave observed in previously reported NLSCNOs with extended polarized and free magnetic layers, our NLSCNO excites a linear propagating spin wave with a constant frequency with increasing excitation currents due to a negligible nonlinearity and Oersted field. Moreover, in conventional NCSTNOs, the current-induced strong local Oersted field dramatically modifies the spin-wave propagation symmetry and results in a highly collimated and single-direction propagation feature due to the opposite propagating path being blocked completely by the strong circular Oersted field-induced corral effect. However, in our NLSCNO, spin waves have bidirectional propagation paths in the direction perpendicular to the external magnetic field because the weak Oersted field-induced corral effect is very limited. Besides, the radial and nonlocal spin current not only excites the auto-oscillation of the nanomagnet under the central nanocontact but can also effectively increase the spin-wave propagation length by spin-torque modulation of spin-wave damping in the outer region of the central nanocontact in our nonlocal geometry. All these

features and the planar geometry improve nonlocal spin-injection devices, which is promising for implementation of nanoscale spin-wave sources for potential magnonics applications and building daisy-chaining oscillatory neural networks for spin wave-based analog computation.

ACKNOWLEDGMENTS

We acknowledge support from the National Key Research and Development Program of China (2016YFA 0300803), the National Natural Science Foundation of China (Grants No. 11774150, No. 12074178, and No. 12004171), the Applied Basic Research Programs of the Science and Technology Commission Foundation of Jiangsu Province (Grant No. BK20200309), the Open Research Fund of Jiangsu Provincial Key Laboratory for Nanotechnology, and the Scientific Foundation of Nanjing University of Posts and Telecommunications (NUPTSF) (Grant No. NY220164).

[1] K. Ando, S. Takahashi, K. Harii, K. Sasage, J. Ieda, S. Maekawa, and E. Saitoh, Electric Manipulation of Spin Relaxation Using the Spin Hall Effect, Phys. Rev. Lett. **101**, 036601 (2008).

[2] V. E. Demidov, S. Urazhdin, E. R. J. Edwards, M. D. Stiles, R. D. McMichael, and S. O. Demokritov, Control of Magnetic Fluctuations by Spin Current, Phys. Rev. Lett. **107**, 107204 (2011).

[3] I. M. Miron, G. Gaudin, S. Auffret, B. Rodmacq, A. Schuhl, S. Pizzini, J. Vogel, and P. Gambardella, Current-driven spin torque induced by the Rashba effect in a ferromagnetic metal layer, Nat. Mater. **9**, 230 (2010).

[4] T. Suzuki, S. Fukami, N. Ishiwata, M. Yamanouchi, S. Ikeda, N. Kasai, and H. Ohno, Current-induced effective field in perpendicularly magnetized Ta/CoFeB/Mgo wire, Appl. Phys. Lett. **98**, 142505 (2011).

[5] L. Q. Liu, C. F. Pai, Y. Li, H. W. Tseng, D. C. Ralph, and R. A. Buhrman, Spin-torque switching with the giant spin Hall effect of tantalum, Science **336**, 555 (2012).

[6] A. R. Mellnik, J. S. Lee, A. Richardella, J. L. Grab, P. J. Mintun, M. H. Fischer, A. Vaezi, A. Manchon, E.-A. Kim, N. Samarth, and D. C. Ralph, Spin transfer torque generated by a topological insulator, Nature **511**, 449 (2014).

[7] F. J. Jedema, A. T. Filip, and B. J. van Wees, Electrical spin injection and accumulation at room temperature in an all-metal mesoscopic spin valve, Nature **410**, 345 (2001).

[8] Y. Ji, A. Hoffmann, J. E. Pearson, and S. D. Bader, Enhanced spin injection polarization in Co/Cu/Co nonlocal lateral spin valves, Appl. Phys. Lett. **88**, 052509 (2006).

[9] T. Kimura, Y. Otani, and J. Hamrle, Switching Magnetization of a Nanoscale Ferromagnetic Particle Using Nonlocal Spin Injection, Phys. Rev. Lett. **96**, 037201 (2006).

[10] T. Yang, T. Kimura, and Y. Otani, Giant spin-accumulation signal and pure spin-current-induced reversible magnetization switching, Nat. Phys. **4**, 851 (2008).

[11] M. Haidar, P. Durrenfeld, M. Ranjbar, M. Balinsky, M. Fazlali, M. Dvornik, R. K. Dumas, S. Khartsev, and J. Akerman, Controlling Gilbert damping in a YIG film using nonlocal spin currents, Phys. Rev. B **94**, 180409(R) (2016).

[12] H. Idzuchi, Y. Fukuma, and Y. Otani, Spin transport in non-magnetic nano-structures induced by non-local spin injection, Physica E **68**, 239 (2015).

[13] P. K. Muduli, O. G. Heinonen, and Johan Akerman, Temperature dependence of linewidth in nanocontact based spin torque oscillators: Effect of multiple oscillatory modes, Phys. Rev. B **86**, 174408 (2012).

[14] R. K. Dumas, E. Iacocca, S. Bonetti, S. R. Sani, S. M. Mohseni, A. Eklund, J. Persson, O. Heinonen, and J. Akerman, Spin-Wave-Mode Coexistence on the Nanoscale: A Consequence of the Oersted-Field-Induced Asymmetric Energy Landscape, Phys. Rev. Lett. **110**, 257202 (2013).

[15] J. Sinova, S. O. Valenzuela, J. Wunderlich, C. H. Back, and T. Jungwirth, Spin Hall effects, Rev. Mod. Phys. **87**, 1213 (2015).

[16] A. Manchon, H. C. Koo, J. Nitta, S. M. Frolov, and R. A. Duine, New perspectives for Rashba spin-orbit coupling, Nat. Mater. **14**, 871 (2015).

[17] A. Hoffmann and S. D. Bader, Opportunities at the Frontiers of Spintronics, Phys. Rev. Appl. **4**, 047001 (2015).

[18] A. Manchon, J. Zelezny, I. M. Miron, T. Jungwirth, J. Sinova, A. Thiaville, K. Garello, and P. Gambardella, Current-induced spin-orbit torques in ferromagnetic and antiferromagnetic systems, Rev. Mod. Phys. **91**, 035004 (2019).

[19] V. E. Demidov, S. Urazhdin, H. Ulrichs, V. Tiberkevich, A. Slavin, D. Baither, G. Schmitz, and S. O. Demokritov, Magnetic nano-oscillator driven by pure spin current, Nat. Mater. **11**, 1028 (2012).

[20] R. H. Liu, W. L. Lim, and S. Urazhdin, Spectral Characteristics of the Microwave Emission by the Spin Hall Nano-Oscillator, Phys. Rev. Lett. **110**, 147601 (2013).

[21] V. E. Demidov, S. Urazhdin, A. Zholud, A. V. Sadovnikov, and S. O. Demokritov, Nanoconstriction-based spin-Hall nano-oscillator, Appl. Phys. Lett. **105**, 172410 (2014).

[22] R. H. Liu, W. L. Lim, and S. Urazhdin, Dynamical Skyrmion State in a Spin Current Nano-Oscillator with Perpendicular Magnetic Anisotropy, Phys. Rev. Lett. **114**, 137201 (2015).

[23] M. Ranjbar, P. Dürrenfeld, M. Haidar, E. Iacocca, M. Balinskiy, T. Q. Le, M. Fazlali, A. Houshang, A. Awad, R. K. Dumas, and J. Åkerman, CoFeB based spin Hall nano-oscillators, IEEE Magn. Lett. **5**, 3000504 (2014).

[24] H. Mazraati, S. Chung, A. Houshang, M. Dvornik, L. Piazza, F. Qejvanaj, S. Jiang, T. Q. Le, J. Weissenrieder, and J. Akerman, Low operational current spin Hall nano-oscillators based on NiFe/W bilayers, Appl. Phys. Lett. **109**, 242402 (2016).

[25] Z. Duan, A. Smith, L. Yang, B. Youngblood, J. Lindner, V. E. Demidov, S. O. Demokritov, and I. N. Krivorotov, Nanowire spin torque oscillator driven by spin orbit torques, Nat. Commun. **5**, 1038 (2014).

[26] M. Collet, X. de Milly, O. d'Allivy Kelly, V. V. Naletov, R. Bernard, P. Bortolotti, J. Ben Youssef, V. E. Demidov, S. O. Demokritov, J. L. Prieto, M. Muñoz, V. Cros, A. Anane, G. de Loubens, and O. Klein, Generation of coherent spin-wave modes in yttrium iron garnet microdiscs by spin-orbit torque, Nat. Commun. **7**, 10377 (2016).

[27] T. Chen, R. K. Dumas, A. Eklund, P. K. Muduli, A. Houshang, A. A. Awad, P. Dürrenfeld, B. G. Malm, A. Rusu, and J. Åkerman, Spin-torque and spin-hall nano-oscillators, Proc. IEEE **104**, 1919 (2016).

[28] V. E. Demidov, S. Urazhdin, G. de Loubens, O. Klein, V. Cros, A. Anane, and S. O. Demokritov, Magnetization oscillations and waves driven by pure spin currents, Phys. Rep. **673**, 1 (2017).

[29] H. Mazraati, S. R. Etesami, S. A. H. Banuazizi, S. Chung, A. Houshang, A. A. Awad, M. Dvornik, and J. Åkerman, Auto-Oscillating Spin-Wave Modes of Constriction-Based Spin Hall Nano-Oscillators in Weak In-Plane Fields, Phys. Rev. Appl. **10**, 054017 (2018).

[30] M. Zahedinejad, A. A. Awad, S. Muralidhar, R. Khymyn, H. Fulara, H. Mazraati, M. Dvornik, and J. Akerman, Two-dimensional mutually synchronized spin Hall nano-oscillator arrays for neuromorphic computing, Nat. Nanotechnol. **15**, 47 (2020).

[31] L. Chen, S. Urazhdin, K. Zhou, Y. W. Du, and R. H. Liu, Magnetic Droplet Mode in a Vertical Nanocontact-Based Spin Hall Nano-Oscillator at Oblique Fields, Phys. Rev. Appl. **13**, 024034 (2020).

[32] L. Li, L. Chen, R. Liu, and Y. Du, Recent progress on excitation and manipulation of spin-waves in spin Hall nano-oscillators, Chin. Phys. B **29**, 117102 (2020).

[33] S. Bonetti, V. Tiberkevich, G. Consolo, G. Finocchio, P. Muduli, F. Mancoff, A. Slavin, and J. Akerman, Experimental Evidence of Self-Localized and Propagating Spin Wave Modes in Obliquely Magnetized Current-Driven Nanocontacts, Phys. Rev. Lett. **105**, 217204 (2010).

[34] A. Houshang, E. Iacocca, P. Durrenfeld, S. R. Sani, J. Akerman, and R. K. Dumas, Spin-wave-beam driven synchronization of nanocontact spin-torque oscillators, Nat. Nanotechnol. **11**, 280 (2016).

[35] V. E. Demidov, S. Urazhdin, and S. O. Demokritov, Direct observation and mapping of spin waves emitted by spin-torque nano-oscillators, Nat. Mater. **9**, 984 (2010).

[36] V. E. Demidov, S. Urazhdin, A. Zholud, A. V. Sadovnikov, A. N. Slavin, and S. O. Demokritov, Spin-current nano-oscillator based on nonlocal spin injection, Sci. Rep. **5**, 8578 (2015).

[37] V. E. Demidov, S. Urazhdin, B. Divinskiy, A. B. Rinkevich, and S. O. Demokritov, Spectral linewidth of spin-current nano-oscillators driven by nonlocal spin injection, Appl. Phys. Lett. **107**, 202402 (2015).

[38] L. Xue, C. Wang, Y.-T. Cui, L. Liu, A. Swander, J. Z. Sun, R. A. Buhrman, and D. C. Ralph, Resonance Measurement of Nonlocal Spin Torque in a Three-Terminal Magnetic Device, Phys. Rev. Lett. **108**, 147201 (2012).

[39] V. E. Demidov, S. Urazhdin, R. H. Liu, B. Divinskiy, A. Telegin, and S. O. Demokritov, Excitation of coherent propagating spin waves by pure spin currents, Nat. Commun. **7**, 10446 (2016).

[40] A. Slavin and V. Tiberkevich, Spin Wave Mode Excited by Spin-Polarized Current in a Magnetic Nanocontact is a Standing Self-Localized Wave Bullet, Phys. Rev. Lett. **95**, 237201 (2005).

[41] Joo-Von Kim, Q. Mistral, C. Chappert, V. Tiberkevich, and A. N. Slavin, Line Shape Distortion in a Nonlinear Auto-Oscillator Near Generation Threshold: Application to Spin-Torque Nano-Oscillators, Phys. Rev. Lett. **100**, 167201 (2008).

[42] A. Slavin and V. Tiberkevich, Excitation of spin waves by spin-polarized current in magnetic nano-structures, IEEE Trans. Magn. **44**, 1916 (2008).

[43] H. Fulara, M. Zahedinejad, R. Khymyn, A. A. Awad, S. Muralidhar, M. Dvornik, and J. Akerman, Spin-orbit torque-driven propagating spin waves, Sci. Adv. **5**, 8467 (2019).

[44] J. C. Slonczewski, Excitation of spin waves by an electric current, J. Magn. Magn. Mater. **195**, L261 (1999).

[45] M. J. Donahue and D. G. Porter, OOMMF (NIST), http://math.nist.gov/oommf.

[46] COMSOL Multiphysics, COMSOL AB, Stockholm, Sweden, www.comsol.com.

[47] M. A. Hoefer, T. J. Silva, and M. D. Stiles, Model for a collimated spin-wave beam generated by a single-layer spin torque nanocontact, Phys. Rev. B **77**, 144401 (2008).